Featured in Physics

Real-Time Trajectory Control of Deterministically Produced Ions

C. Lopez, A. Trimeche, D. Comparat, and Y.J. Picard*
Laboratoire Aimé Cotton, CNRS, Université Paris-Sud, ENS Paris Saclay, Université Paris-Saclay, Bâtiment 505, 91405 Orsay, France

(Received 20 December 2018; revised manuscript received 25 March 2019; published 21 June 2019)

The major challenge to improve deterministic single-ion sources is to control the position and momentum of each ion. On the basis of the extra information given by the electron created in a photoionization process, the trajectory of the correlated ion can be corrected with use of a fast real-time feedback system. In this paper, we report on a proof-of-principle experiment that demonstrates the performance of this feedback control with individual cesium ions. The electron produced is detected with a time- and position-sensitive detector, the information from which is used to quickly infer the position of the corresponding ion. Then the feedback system drives the ion trajectory through steering plates, and the individual ion can thus be sent to any dedicated location. This enables us to perform deterministic patterning and achieve a factor-of-1000 reduction in spot area. The single-ion feedback control is versatile and can be applied to different kinds of ion sources. It provides a powerful tool to optimize the ion beam and offers a complete portfolio for quantum systems and applications in materials science.

DOI: 10.1103/PhysRevApplied.11.064049

I. INTRODUCTION

The preparation and handling of individual particles is crucial for new technology development. Deterministic and high-precision placement of individual atoms and ions offers exciting prospects for the realization of quantum-based devices at the nanoscale [1,2]. Several mechanisms for the manipulation of individual atoms and ions have been demonstrated [3–5], but they are usually slow and nondeterministic. Recently, new types of ion sources have emerged: these are based either on cold trapped ions [6,7] or cold trapped atoms that are subsequently photoionized [8]. From trapped ions, deterministic sources and implantation of several types of ions with down to 6-nm resolution have been demonstrated but the repetition rate and the beam energy range have still to be increased [7,9,10]. By ionization of cold atoms, a very-high-current and high-brightness beam can be produced but with a nondeterministic property [11,12]. Progress toward deterministic production of single ions has been made by exploiting the correlation between an electron and the associated ion after photoionization of cold trapped rubidium atoms [13] or an atomic beam [14]. The electron heralds the creation of a corresponding ion. As stressed in Refs. [13,14], the next step would be to extend the scheme beyond time-correlated feedback to have a position- and momentum-correlated feedback so as to provide total control over each single ion in a beam. This would provide general and powerful tools to optimize the ion beam and would offer a complete portfolio for quantum optics and applications in materials science.

This position-correlated feedback is exactly the step that we demonstrate in this paper. We exploit the correlation between an electron and the associated ion created by photoionization of an atom. We use fast real-time feedback to modify the ion trajectory on the basis of information obtained by direct detection of the electron. We demonstrate an active correction of the trajectory allowing the ion to be sent to any desired final location independently of its initial position. This allows full control of the final spot pattern with increased accuracy compared with the uncorrected one, which enables us to reduce the ultimate achievable spot size by correcting each ion trajectory. A 3-orders-of-magnitude reduction in spot area is demonstrated in a one-by-one ion-driving experiment on a millimeter-initial-size ion spot. In principle this reduction remains valid even if we start from a micrometer spot size. In this case the nanometer scale is probably reachable with use of, for instance, a focused-ion-beam (FIB) column. This trajectory correction can be generalized to control all beam parameters (position, momentum, energy), and thus can greatly increase the phase-space density, the brightness and the emittance of the ion beam. In this paper we focus only on basic correction schemes consisting of the correction of the ion position on the target detector and the application of a virtual diaphragm and mask. In the following, we first present the apparatus. We then study the correlation between electrons and ions. Finally, we present the results of the feedback correction allowing us to create any patterns of ion spots.

*yan.picard@u-psud.fr

II. EXPERIMENTAL SETUP

A. Ionization and extraction

The setup is based on a double-time-of-flight (TOF) spectrometer with time- and position-sensitive detectors (TPSD) at opposite ends monitored in coincidence mode (see Fig. 1). For our experiment, we use cesium (Cs) atoms so as to create ion-electron pairs. Cs effuses from an oven and passes through a 3-mm-diameter and 10-cm-long heated copper tube, and then propagates 20 cm to the ionization region. Photoionization is performed in a quasi-uniform static electric field produced in between two holed electrodes (4-mm hole diameter) separated by 10 mm. By use of narrowband lasers for the photoionization, Doppler selection can be performed to reduce drastically the effect of the effusive atomic beam velocity dispersion. Ionization of Cs atoms is performed with a three-photon transition process, where the first transition uses a horizontal laser beam counterpropagating with respect to the atomic beam. It is ensured by a 852-nm laser beam that excites atoms from the $6S_{1/2}$ $F = 4$ level to the $6P_{3/2}$ $F = 5$ level. For Doppler compensation, this laser is locked by saturated absorption on a vapor cell and detuned by an acoustic optical modulator. The second transition is performed by a perpendicular 1470-nm laser beam coupling the excited $6P_{3/2}$ state to the $7S_{1/2}$ state. This laser is locked by means of a Cs cell excited by the 852-nm laser. The last transition is ensured by a tunable Ti:sapphire laser in the same plane but tilted 45° from the previous lasers. It excites the atoms from the $7S_{1/2}$ state to a Rydberg state or the ionization continuum depending on the wavelength chosen (770–795 nm). This geometry enables us to control the ionization volume at the crossing of the laser beams. These lasers are focused, inside the extraction zone, with a typical size of approximately 500 μm. For the results presented here, ionization occurs in a 2200 V/cm field and the (vacuum) Ti:sapphire-laser wavelength is tuned to 794.432 nm. Fine adjustments are made to the Ti:sapphire-laser wavelength to optimize the detected electron and ion signals. We choose this wavelength because it results in efficient excitation to a Rydberg state that autoionizes, and produces an efficient source of ion and electron pairs. On ionization, electrons and ions are accelerated by the 2200 V/cm static electric field in opposite directions toward the TPSD located 355 mm (for electrons) and 285 mm (for ions) from the ionization region. Typical TOF values are about 20 ns for electrons and 7 μs for ions. Outside the ionization region, along the ion trajectory, a set of horizontal and vertical deflection plates are dedicated to the ion-trajectory correction.

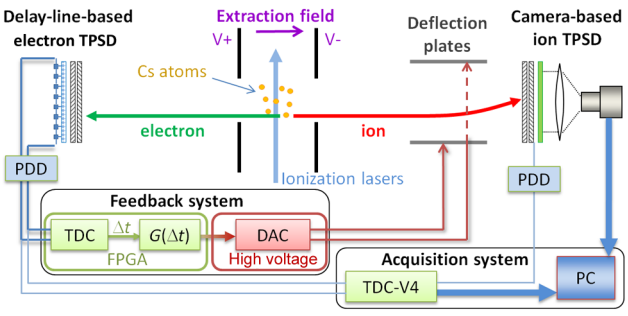

FIG. 1. Experimental setup. Electrons and ions, produced by photoionization of a cesium beam, are extracted in opposite directions and detected by two TPSDs. The acquisition system handles the information from the detectors and processes the data. The feedback system controls the ion trajectory by acting on the deflection plates with the appropriate voltages for each ion (presented here in one dimension; see the text for more details). DAC, digital-to-analog converter.

B. Detection and acquisition

To reveal the correlation between an electron and an ion and use it to infer the ion position, we need to determine the position and TOF of both particles. For this, we use two TPSDs monitored in coincidence mode by an acquisition system that works independently of the fast feedback system (see Fig. 1). The electron TPSD is composed by a set of imaging-quality microchannel plates (MCPs) and a delay-line detector (DLD). The DLD is based on capacitive coupling between a resistive anode, which collects the electron cloud arising from the MCP, and an encoding surface through a ceramic plate [15]. This detector has a position resolution of about 50 μm. The two pairs of analog signals coming from X (horizontal) and Y (vertical) delay lines pass through homemade fast amplifiers and peak-detection discriminators (PDDs) [16] that deliver short (approximately 15 ns) logical signals. These signals end in a multichannel time-to-digital converter (TDC; TDC-V4 [17]) with a resolution of 60 ps (rms). The ion TPSD is composed of a set of imaging-quality MCPs, a phosphor screen, and a CMOS camera. It is based on correlation between the brightness of the spot on the phosphor screen and the amplitude of the time signal on the MCP [18]. This detector has a position resolution of about 50 μm. The two time signals for the ion and the electron generated by the MCP are digitized by the PDDs and recorded by the TDC-V4 time-to-digital converter. This enables us to measure the relative TOF of the detected ion and electron. The time and position signals delivered by the two TPSDs are handled by a C++ monitoring home-written program that controls acquisition and stores the data. For each detected event, the acquisition program determines the position and relative TOF of the ion and the electron. If this TOF fits in a given range (approximately 200 ns, corresponding to the spread caused by the potential difference across the ionization region) around the expected value, the pair is considered as coming from a unique ionization event and is labeled coincident in time. This is

a mandatory condition to obtain electron-ion correlation. For this proof-of-principle experiment, a low counting rate (approximately 1 kHz) is chosen so as to be compatible with the acquisition rate of the CMOS camera. This rate ensures that the false coincidences are negligible and that the correction by the steering plates never concerns more than one ion.

The acquisition system is used to characterize the correlation between the two particles produced by the ionization. Figure 2 shows typical correlation between individual ions and electrons arising from all the validated coincident events. Images of all electrons and ions detected in coincidence are shown in Figs. 2(a) and 2(b), respectively, for several thousand acquisition events. For each coincident event, the X (Y) coordinate of the electron is plotted with respect to the X (Y) coordinate of the corresponding ion on the correlation map shown in Fig. 2(c) [Fig. 2(d)]. These maps show two narrow correlation patterns on each coordinate. The slight curvature of these correlation patterns is due to aberrations such as that induced by the residual magnetic fields seen by the electrons during their flight. Hence, for each detected electron, and from the measurement of its position, we can deduce the position of the coincident ion. The correlation pattern must be one-to-one (injective), and its width limits the precision of the inferred position of the ion. This width is mainly affected by nonzero electron-emission energy, ion-velocity spread, extracting-field inhomogeneity, and a variety of other minor factors, such as

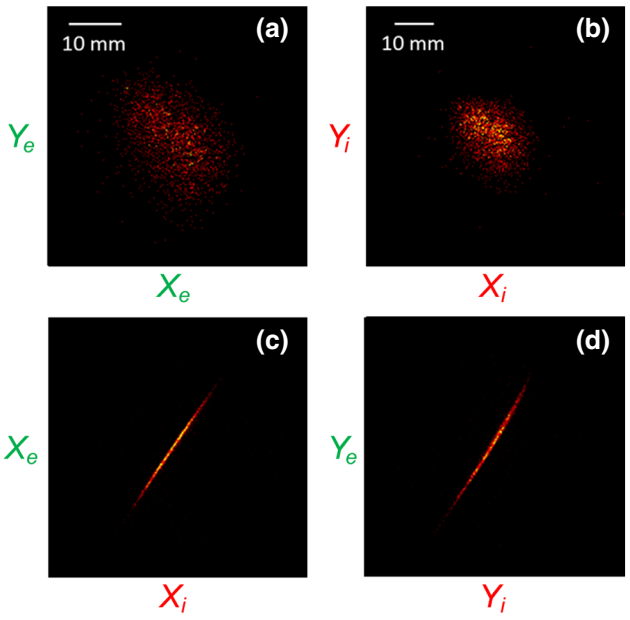

FIG. 2. (a),(b) Raw images from the position-sensitive detectors of electrons (X_e,Y_e) and ions (X_i,Y_i), respectively; (c),(d) Correlation patterns between, respectively, the horizontal and vertical coordinates of the coincident events. The position scales are shown in (a) for (X_e,Y_e) and in (b) for (X_i,Y_i) and are the same for all images in this paper.

fluctuation of the fields affecting the trajectories and the resolution of the electron detector. The main factors are overcome, respectively, by threshold ionization (electron-emission energy on the order of a few millielectronvolts), Doppler selection (ion-velocity spread on the order of a few meters per second), and spatially resolved Rybdberg-state excitation inside the ionization zone (giving a spatial ionization width of 10–100 μm).

C. Fast feedback system

The fast determination of the detected electron position allows us to perform active feedback control in real time for each ion trajectory. The feedback system gets the X and Y coordinates of the electron from the DLD and processes them to apply the correction by sending appropriate voltages onto the four deflection plates. In more detail, copies of the logical signals arising from the DLD are sent to a field-programmable gate array (FPGA) [19,20] that manages the feedback calculation. The feedback parameters (such as the transfer functions) are then experimentally optimized. Inside this integrated circuit, four TDCs measure the arrival time of each signal. The TDCs are of tapped-delay-line type [21] with a standard deviation of approximately 75 ps. Thus, a finite-state machine within the FPGA checks the validity of each event. If it gets the four expected signals from the DLD during a window corresponding to the delay-line propagation time (approximately 80 ns), the event is validated. If not, multiple hits or incomplete hits are ignored. Once the event is validated, the X and Y coordinates of the electron are extracted from the time difference Δt of each pair of signals and are processed by two transfer functions $G(\Delta t)$ (see Fig. 1) to deliver the correction we wish to apply. After this FPGA calculation, a high-speed isolated serializer transfers numerical data to a high-voltage electronic board with a delay of 400 ns. On this board, four digital-to-analog converters with amplifiers generate the appropriate voltages (offset voltage pulses of a few tens of volts for a few microseconds) to supply the steering plates, with a transition time on the order of microseconds. The correlated ion reaches the deflection plates after a TOF of approximately 3 μs, which is longer than the transition time of the voltage pulses. When the ion is in between the steering plates, the applied correction voltages deflect its trajectory according to the feedback-system instructions. Additionally, to enhance the deterministic behavior of our source, we set by default the deflectors in a configuration where the ions are permanently steered out from the target, except when an electron is validated by the feedback system, which then lets the correlated ion pass through with the adequate correction.

III. RESULTS AND DISCUSSION

Figure 3 shows the key control configurations we apply to verify the validity of our approach and to demonstrate

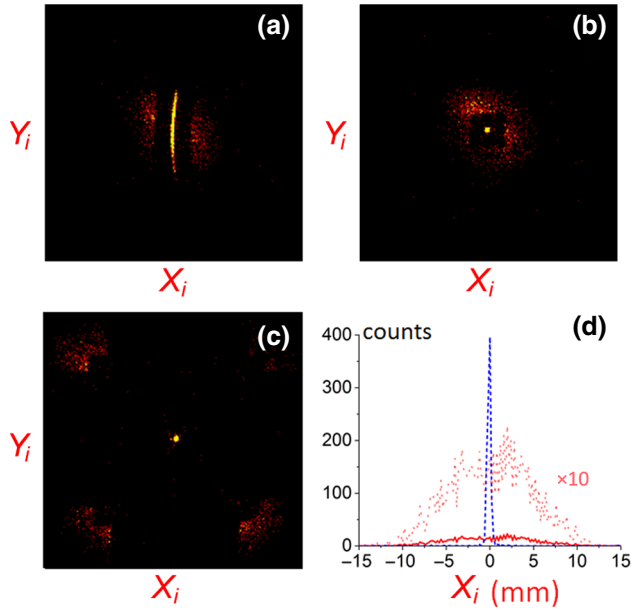

FIG. 3. Raw images from the ion detector after (a) 1D correction along the X direction on a selected zone, (b) 2D correction on a selected zone, and (c) 2D correction with nonselected ions performed of the target. (d) Projection on the X axis of the ion-position distribution without correction (solid red line, and red dots for amplitude $\times 10$) and with 2D correction (dashed blue line). The FWHM is reduced by a factor of approximately 30 in each direction.

the performance of our feedback system. Figure 3(a) presents an image of the detected ions after application of a one-dimensional (1D) correction on the X axis. As can be seen, the corrected ions are aligned along the Y direction. Here a simple linear transfer function $G(\Delta t)$ is set along the X component so that each ion is carried onto a vertical line when it reaches the target detector. The slight curvature seen in the resulting structure is due to the nonlinearity of the correlation patterns. As mentioned before, this nonlinearity is mainly caused by the residual magnetic field. The feedback system could correct this curvature, but for this paper we ignore it and show a simple way to bypass it by applying a virtual diaphragm that selects the quasilinear part. Figure 3(b) shows an image of the detected ions after application of a two-dimensional (2D) correction on the X axis and Y axis. As can be seen, the corrected ions are sent to a very small spot on the target detector. This spot is much smaller than we obtain at best by focusing with our electrostatic lenses because of the one-by-one ion-trajectory correction. A nonlinear correction is very possible with this feedback system. This will lead to an even smaller spot, but it is beyond the scope of this paper. In these experiments we select a 1D zone [Fig. 3(a)] or a 2D zone [Fig. 3(b)] in which we apply the correction. If the validated electron coordinate X or Y is inside the zone of interest, the steering voltages are set to the appropriate values to correct the ion trajectory. If the electron coordinate is outside the zone of interest, these voltages are set to zero so that the ion passes through without deviation. An interesting alternative is to push out this nonselected ion. Figure 3(c) shows an experimental result for this configuration, where we can see at the center of the image the spot formed by the corrected ions and at the edges of the image the pushed ions. Here we do not push out the nonselected ions very far from the zone of interest so as to see them, but we can easily drive them far away from the detector target. This corresponds to adding a virtual diaphragm to the correction process. Figure 3(d) shows the profile of the ion spots with and without correction. It demonstrates a reduction by a factor of 30 of the spot width. The same result is obtained on the other axis, which gives a 3-orders-of-magnitude reduction in the ion spot area after correction. By numerically simulating the correction, using the raw data from the acquisition system without correction, we obtain the same result, which means that this reduction factor is more limited by the width of the correlation pattern than by the feedback-system accuracy. The virtual-diaphragm functionality is thus very useful. For instance, when the width of the correlation pattern is not uniform, we can select a zone with the thinnest width in which we apply the correction and remove the nonselected ions. This leads to an improvement of the correction quality without a large current loss. This virtual mask enables us also to select a zone which corresponds to a very small part of the ionization region so as to minimize the effect of the energy spread and aberrations.

Our feedback system is versatile and allows us to realize more-complex processes. Figure 4(a) shows an example of a complex pattern that can be produced, where the selected ions are carried on to three different spots as a function of the position of their correlated electrons. Here the selected zone is separated into a 2×3 array, but more-complex patterns can easily be obtained by use of larger arrays. Indeed, we can draw any desired form on the target with the corrected ions. As we see in Fig. 3(c), the feedback system can play the role of a diaphragm. With a more-complex selected zone, and without correction on the selected ions, the feedback system can also play the role of a mask. An example of such a mask is shown in Fig. 4(b), where a 16×16 array mask implemented in the FPGA is represented in the upper-left corner; the selected ions corresponding to the green (white) pixels are placed at position 1 (position 2) on the detector target; the nonselected ions are pushed away to position 3. Note that the structures (1, 2, 3) are accumulated during the same experiment and are all kept inside the detector target for demonstration purposes. Obviously, if we couple a correction of the selected ions with this kind of virtual mask, we can drive single ions to any desired location and realize any conceivable pattern on the target.

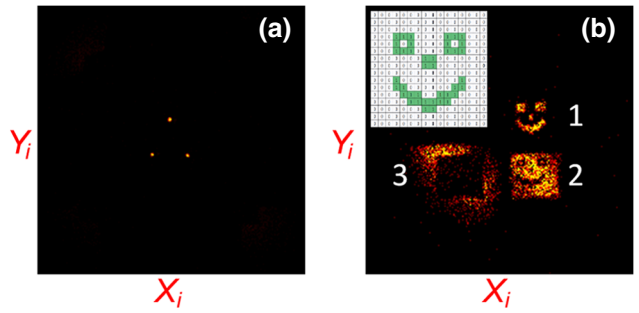

FIG. 4. Raw images from the ion detector after (a) application of a 2D correction in which the ions are carried on to three different spots at the target and (b) application of a virtual mask implemented in the FPGA.

IV. CONCLUSION

In conclusion, by using the correlation between an ion and an electron, produced by photoionization of an atomic beam, we develop a fast feedback system to control the ion trajectory. Compared with previous Rb-photoionization experiments [13,14] we add, to the deterministic character of the ion delivery, the control of its trajectory and complex patterning such as multiple spots and a virtual diaphragm or mask. The focusing performance of our system is better than that obtained with conventional lenses due to the one-by-one ion-trajectory correction. This correction method is quite general and can be implemented in different setups, and the feedback can be applied not only to a steering plate but also to any electromagnetic components that affect the ion trajectory (grids, lenses, prisms, etc.). This feedback system can even correct more-complex effects such as finite source size, electrostatic or magnetic lens aberrations, and stray fields by application of nonlinear and/or individually adapted corrections for each ion. In principle, such a system can be used in reverse mode to control the electron instead of the ion. This requires only a dedicated (acceleration-deceleration) geometry that ensures the detection of the ion before the electron. This proof-of-principle experiment is performed with a millimeter-scale ion source that is downsized to micrometer scale on the target at a repetition rate of approximately 1 kHz. Coupled with the appropriate setup, this feedback system may produce a 10-MHz-rate (1-pA) beam by reducing the ion TOF inside the steering plates and increasing the capacity of the detector to handle high count rates. Numerous methods, such as discreet-anode detectors, coherent excitation processes, and Rydberg dipole blockade, can probably be used to increase the rate even further [22,23]. Spectacular increase of the final spot resolution can be also achieved with an FIB column based on direct photoionization or excitation of field-ionized Rydberg states of ultracold atoms [8,11]. This allows a drastic reduction of the initial ion velocities, leading to a very narrow ion-electron correlation pattern. Preliminary simulations prove that our feedback system can produce subnanometer spots even for quite low beam energy since we correct each ion independently. The deterministic behavior and complex patterning obtained by this feedback method makes it very useful for FIB studies such as for nanostructuring, microscopy, and surface spectroscopy [24,25]. It can be used in future semiconductor fabrication or in quantum-technology development, for instance, by structuring devices at an unprecedented precision [2,26]. Hence, this feedback method can be used in ion-beam techniques such as aberration correction, high-resolution imaging, and accurate implantation.

ACKNOWLEDGMENTS

This work was supported by the Fonds Unique Interministériel (IAPP-FUI-22) project ColdFIB, the European Research Council under Grant Agreement No. 712718-LASFIB, ANR HREELM, and CEFIPRA (Grant No. 5404-1). The authors thank G. Chaplier and DTPI for useful help in developing the detectors and L. Calmon for her contribution in numerical simulations.

[1] Bharat Bhushan, *Springer Handbook of Nanotechnology* (Springer, Berlin, Heidelberg, 2017).

[2] David N. Jamieson, William I. L. Lawrie, Simon G. Robson, Alexander M. Jakob, Brett C. Johnson, and Jeffrey C. McCallum, Deterministic doping, Mater. Sci. Semicond. Process. **62**, 23 (2017).

[3] Donald M. Eigler and Erhard K. Schweizer, Positioning single atoms with a scanning tunnelling microscope, Nature **344**, 524 (1990).

[4] M. Hori, T. Shinada, K. Taira, N. Shimamoto, T. Tanii, T. Endo, and I. Ohdomari, Performance enhancement of semiconductor devices by control of discrete dopant distribution, Nanotechnology **20**, 365205 (2009).

[5] Johannes V. Barth, Giovanni Costantini, and Klaus Kern, in *Nanoscience and Technology: A Collection of Reviews from Nature Journals* (World Scientific, 2010), p. 67.

[6] W. Schnitzler, N. M. Linke, R. Fickler, J. Meijer, F. Schmidt-Kaler, and K. Singer, Deterministic Ultracold Ion Source Targeting the Heisenberg Limit, Phys. Rev. Lett. **102**, 70501 (2009).

[7] F. Schmidt-Kaler, G. Jakob, K. Groot-Berning, K. Singer, and U. Poschinger, in *Quantum Information and Measurement* (Optical Society of America, Mainz, 2017), p. QW3A.

[8] J. J. McClelland, A. V. Steele, B. Knuffman, K. A. Twedt, A. Schwarzkopf, and T. M. Wilson, Bright focused ion beam sources based on laser-cooled atoms, Appl. Phys. Rev. 3, 011302 (2016), arXiv:1510.08673 [physics.atom-ph].

[9] Georg Jacob, Karin Groot-Berning, Sebastian Wolf, Stefan Ulm, Luc Couturier, Samuel T. Dawkins, Ulrich G. Poschinger, Ferdinand Schmidt-Kaler, and Kilian Singer,

Transmission Microscopy with Nanometer Resolution Using a Deterministic Single Ion Source, Phys. Rev. Lett. **117**, 043001 (2016).

[10] Karin Groot-Berning, Thomas Kornher, Georg Jacob, Felix Stopp, Samuel T. Dawkins, Roman Kolesov, and Ferdinand Schmidt-Kaler, Deterministic single ion implantation of rare-earth ions for nanometer resolution colour center generation, arXiv:1902.05308 (2019).

[11] M. Viteau, M. Reveillard, L. Kime, B. Rasser, P. Sudraud, Y. Bruneau, G. Khalili, P. Pillet, D. Comparat, I. Guerri, A. Fioretti, D. Ciampini, M. Allegrini, and F. Fuso, Ion microscopy based on laser-cooled cesium atoms, Ultramicroscopy **164**, 70 (2016).

[12] Adam V. Steele, Andrew Schwarzkopf, Jabez J. McClelland, and Brenton Knuffman, High-brightness Cs focused ion beam from a cold-atomic-beam ion source, Nano Futures **1**, 015005 (2017).

[13] Cihan Sahin, Philipp Geppert, Andreas Müllers, and Herwig Ott, A high repetition deterministic single ion source, New J. Phys. **19**, 123005 (2017).

[14] A. J. McCulloch, R. W. Speirs, S. H. Wissenberg, R. P. M. Tielen, B. M. Sparkes, and R. E. Scholten, Heralded ions via ionization coincidence, Phys. Rev. A **97**, 043423 (2018).

[15] D. Céolin, G. Chaplier, M. Lemonnier, G. A. Garcia, C. Miron, L. Nahon, M. Simon, N. Leclercq, and Pascal Morin, High spatial resolution two-dimensional position sensitive detector for the performance of coincidence experiments, Rev. Sci. Instrum. **76**, 043302 (2005).

[16] DTPI, ISMO/LUMAT, CNRS/Université Paris-Sud/IOGS/Université Paris-Saclay, Orsay, France.

[17] DTPI: https://www.pluginlabs-universiteparissaclay.fr/fr/entity/917038-dtpi-detection-temps-position-image.

[18] Xavier Urbain, D. Bech, J.-P. Van Roy, M. Géléoc, S. J. Weber, A. Huetz, and Y. J. Picard, A zero dead-time multi-particle time and position sensitive detector based on correlation between brightness and amplitude, Rev. Sci. Instrum. **86**, 023305 (2015).

[19] S. Trimberger, D. Carberry, A. Johnson, and J. Wong, in *Proceedings. The 5th Annual IEEE Symposium on Field-Programmable Custom Computing Machines Cat. No.97TB100186)* (IEEE, San Jose, 1997), p. 22.

[20] E. Monmasson and M. N. Cirstea, FPGA design methodology for industrial control systems – a review, IEEE Trans. Ind. Electron. **54**, 1824 (2007).

[21] Claudio Favi and Edoardo Charbon, in *Proceedings of the ACM/SIGDA International Symposium on Field Programmable Gate Arrays* (ACM, Lausanne, 2009), p. 113.

[22] I. I. Beterov, D. B. Tretyakov, V. M. Entin, E. A. Yakshina, I. I. Ryabtsev, C. MacCormick, and S. Bergamini, Deterministic single-atom excitation via adiabatic passage and Rydberg blockade, Phys. Rev. A **84**, 023413 (2011).

[23] B. M. Sparkes, D. Murphy, R. J. Taylor, R. W. Speirs, A. J. McCulloch, and R. E. Scholten, Stimulated Raman adiabatic passage for improved performance of a cold-atom electron and ion source, Phys. Rev. A **94**, 023404 (2016).

[24] Jon Orloff, *Handbook of Charged Particle Optics* (CRC Press, Boca Raton, 2008).

[25] Jacques Gierak, Focused ion beam technology and ultimate applications, Semicond. Sci. Technol. **24**, 43001 (2009).

[26] Guilherme Tosi, Fahd A. Mohiyaddin, Vivien Schmitt, Stefanie Tenberg, Rajib Rahman, Gerhard Klimeck, and Andrea Morello, Silicon quantum processor with robust long-distance qubit couplings, Nat. Commun. **8**, 450 (2017).